# Thieno[3,4-c]pyrrole-4,6-dione-Based Polymer Semiconductors: Toward High-Performance, Air-Stable Organic Thin-Film Transistors

**ARTICLE** *in* JOURNAL OF THE AMERICAN CHEMICAL SOCIETY · AUGUST 2011

Impact Factor: 12.11 · DOI: 10.1021/ja205398u · Source: PubMed



**9 AUTHORS**, INCLUDING:

Xugang Guo
South University of Science and Technology …
**28** PUBLICATIONS **1,570** CITATIONS
SEE PROFILE

Rocio Ponce Ortiz
University of Malaga
**69** PUBLICATIONS **2,438** CITATIONS
SEE PROFILE

Shiming Zhang
Huawei Technologies Co. Ltd.
**20** PUBLICATIONS **774** CITATIONS
SEE PROFILE

Antonio Facchetti
Northwestern University
**381** PUBLICATIONS **22,191** CITATIONS
SEE PROFILE

JACS
JOURNAL OF THE AMERICAN CHEMICAL SOCIETY

ARTICLE

pubs.acs.org/JACS

# Thieno[3,4-*c*]pyrrole-4,6-dione-Based Polymer Semiconductors: Toward High-Performance, Air-Stable Organic Thin-Film Transistors

Xugang Guo,[†] Rocio Ponce Ortiz,[†,‡] Yan Zheng,[§] Myung-Gil Kim,[†] Shiming Zhang,[†] Yan Hu,[§] Gang Lu,[†] Antonio Facchetti,*[,†,§] and Tobin J. Marks*[,†]

[†]Department of Chemistry and the Materials Research Center, Northwestern University, 2145 Sheridan Road, Evanston, Illinois 60208, United States

[‡]Department of Physical Chemistry, University of Málaga, Campus de Teatinos s/n, Málaga 29071, Spain

[§]Polyera Corporation, 8045 Lamon Avenue, Skokie, Illinois 60077, United States

Supporting Information

**ABSTRACT:** We report a new p-type semiconducting polymer family based on the thieno[3,4-*c*]pyrrole-4,6-dione (TPD) building block, which exhibits good processability as well as good mobility and lifetime stability in thin-film transistors (TFTs). TPD homopolymer **P1** was synthesized via Yamamoto coupling, whereas copolymers **P2**−**P8** were synthesized via Stille coupling. All of these polymers were characterized by chemical analysis as well as thermal analysis, optical spectroscopy, and cyclic voltammetry. **P2**−**P7** have lower-lying HOMOs than does P3HT by 0.24−0.57 eV, depending on the donor counits, and exhibit large oscillator strengths in the visible region with similar optical band gaps throughout the series (∼1.80 eV). The electron-rich character of the dialkoxybithiophene counits in **P8** greatly compresses the band gap, resulting in the lowest $E_g^{opt}$ in the series (1.66 eV), but also raising the HOMO energy to −5.11 eV. Organic thin-film transistor (OTFT) electrical characterization indicates that device performance is very sensitive to the oligothiophene conjugation length, but also to the solubilizing side chain substituents (length, positional pattern). The corresponding thin-film microstructures and morphologies were investigated by XRD and AFM to correlate with the OTFT performance. By strategically varying the oligothiophene donor conjugation length and optimizing the solubilizing side chains, a maximum OTFT hole mobility of ∼0.6 $cm^2 V^{-1} s^{-1}$ is achieved for **P4**-based devices. OTFT environmental (storage) and operational (bias) stability in ambient was investigated, and enhanced performance is observed due to the low-lying HOMOs. These results indicate that the TPD is an excellent building block for constructing high-performance polymers for p-type transistor applications due to the excellent processability, substantial hole mobility, and good device stability.

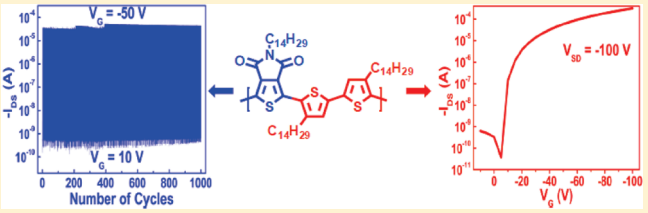


## INTRODUCTION

Benefiting from new materials development,[1−8] as well as optimized processing and device fabrication,[9−12] the performance of organic thin-film transistors (OTFTs) based on polymeric semiconductors has advanced dramatically during the past decade, with the charge carrier mobility ($\mu$) now approaching/surpassing 1 $cm^2 V^{-1} s^{-1}$.[3−6,8,9,11,13−15] Such performance is comparable to that of hydrogenated amorphous silicon (a-Si:H), opening enormous opportunities for the fabrication of cost-effective, flexible electronics.[16−19] However, many applications of organic semiconductors are currently limited by OTFT performance degradation on prolonged exposure to ambient atmosphere and/or operation under bias.[1,13,20] With few exceptions,[2,21−25] large carrier mobilities and stable operation for polymer semiconductor OTFTs are typically achieved in low-humidity or inert atmosphere.[1,3,9,13,14,26−29] Most reported examples of enhanced device air stability are typically based on ambient exposure data in the absence of bias. For applications in low-end products, such as radio frequency identification cards (RFID)[30,31] and sensors,[32,33] current storage stability levels may be sufficient, and operational stability under bias does not seem critical.[17] However, for large-scale high-technology applications such as display drivers and logic circuitry, both the storage and the operational stability under ambient storage and bias are essential and have come under more intense scrutiny.[17,31] As the carrier mobility of polymer semiconductors approaches or surpasses that of a-Si:H, realizing new high-performance materials having large carrier mobilities and robust operational stability in the ambient becomes an important scientific and technological goal.

As an emerging electron-deficient materials building block, thieno[3,4-*c*]pyrrole-4,6-dione (TPD) has received much attention in low band gap donor−acceptor (D−A) copolymers for high-performance organic photovoltaic (OPV) devices.[34−45] The electron-deficient character of TPD greatly lowers the HOMOs of the corresponding copolymers, affording high open

**Received:** June 10, 2011
**Published:** July 26, 2011

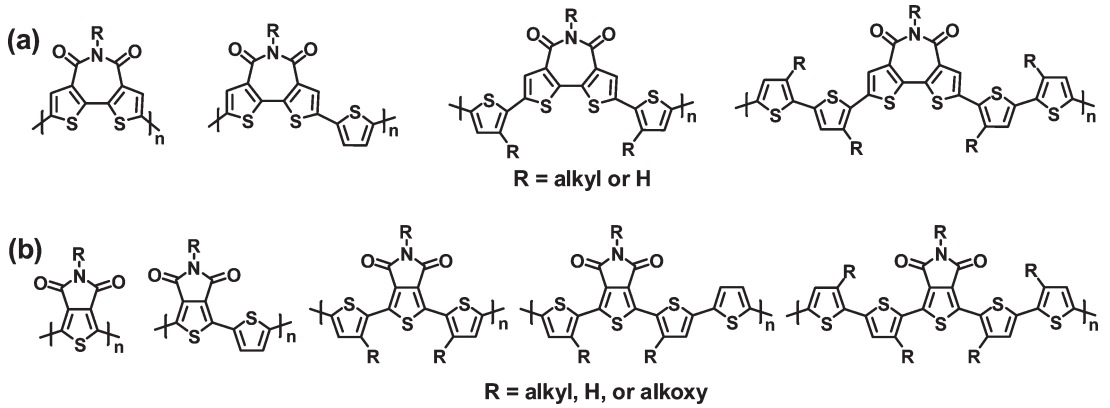


**Figure 1.** Chemical structures of bithiophene imide (BTI)-based polymer semiconductors (a) reported previously[50,51] and thieno[3,4-*c*]pyrrole-4, 6-dione (TPD)-based polymer semiconductors (b) reported in this work.

**Scheme 1. Synthetic Routes to TPD Monomers 3 and TPD Derivatives 5 with Flanked Thiophenes for TPD-Based Polymer Synthesis**[a]

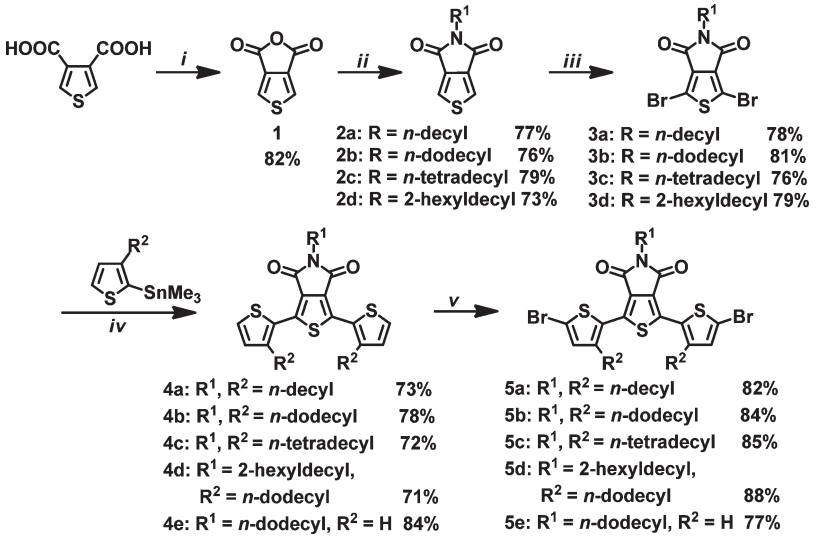


[a] Reagent and conditions: (i) $Ac_2O$, 140 °C; (ii) (a) $R^1NH_2$, toluene, reflux; (b) $SOCl_2$, reflux; (iii) NBS, $H_2SO_4$, $CF_3COOH$, room temperature; (iv) $Pd(PPh_3)Cl_2$ (0.1 equiv), THF, 80 °C; (v) $Br_2$, $CHCl_3$, AcOH, room temperature.

circuit voltages (0.8−1.0 V) and excellent OPV power conversion efficiencies (3−7%).[34−45] However, TPD has not been successfully introduced into high-performance OTFT polymers, and reported hole mobilities are unfortunately below 0.01 $cm^2\ V^{-1}\ s^{-1}$.[40−42] For OTFT applications, low-lying HOMOs are essential to resist air oxidation and thus increase device stability.[46−48] However, if the HOMO energy is too low, the resulting barrier to hole injection may compromise device performance. Thus, a delicate balance between these two effects must be achieved.[49]

Recently, we reported on a bithiophene imide (BTI, Figure 1a)-based polymer series designed for OTFTs.[51] The BTI electron deficiency lowers the HOMO energies of the resulting polymers, and incorporation of oligothiophene comonomers leads to moderate hole mobilities and enhanced device storage stability. As compared to the BTI building block,[50] TPD is far easier to synthesize,[52] and the resulting polymers can exhibit superior solubility/processability due to the fused structures of the BTI units. Furthermore, DFT computations (see the Supporting Information) indicate that alkyl functionalization at the thiophene 3-position adjacent to the TPD units affords a coplanar geometry, which is enforced by attractive (thienyl)-S···O(carbonyl) interactions.[53−56] Thus, while the sum of S and O van der Waals radii is 3.32 Å, DFT calculations on thiophene−TPD−thiophene molecules yield a significantly shorter S···O distance (2.89 Å), indicating significant S···O interactions (Figure S36). Here, we report the synthesis and characterization of a new series of TPD-based D−A copolymers having variable conjugation length alkyl/alkoxy-functionalized oligothiophene donor counits functionalized with solubilizing side chains of varying dimensions, with the goal of achieving high-performance polymer semiconductors for applications in OTFTs having enhanced environmental and bias stability. It will be seen that variation of donor counits affords broadly tunable HOMO energies, optimized film microstructures and morphologies, and, hence, broadly tunable OTFT performance. We characterize here device stability under both storage and bias in ambient. The results indicate that by implementing the

**Scheme 2. Synthesis of BTI-Based Homopolymers and Copolymers**[a]

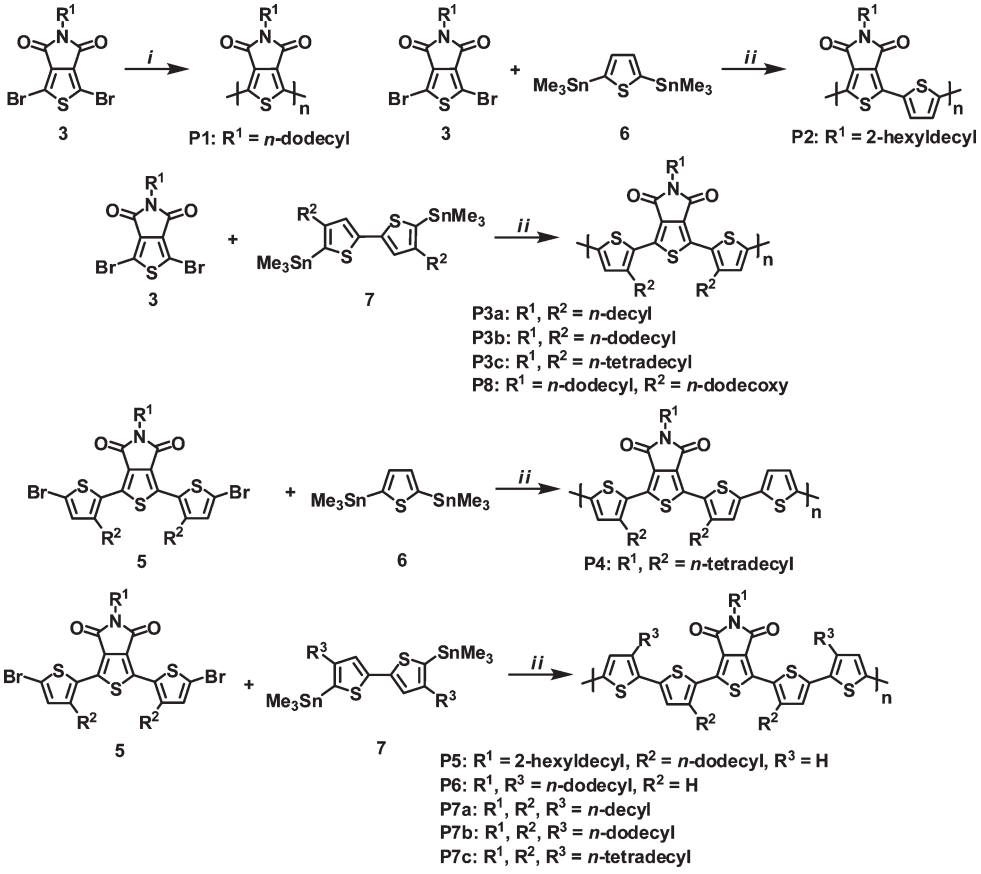


[a] Reagent and conditions: (i) $Ni(COD)_2$, COD, DMF, 2,2′-bipy, 80 °C; (ii) $Pd_2(dba)_3$, P(*o*-tolyl)$_3$ [1:8, $Pd_2(dba)_3$:P(*o*-tolyl)$_3$ molar ratio; Pd loading 0.03−0.05 equiv], toluene, 110 °C.

electron-deficient properties of TPD, we are able to tune the semiconductor HOMO levels and achieve good OTFT storage and operational stability.

## RESULTS AND DISCUSSION

In this section, we first discuss building block and polymer syntheses, followed by their characterization using NMR, GPC, EA, XPS, DSC, optical spectroscopy, and electrochemistry in solution and/or in the solid state. Next, thin-film transistors are fabricated, followed by electrical measurements and investigations of device stability. Properties of the polymer thin films are also characterized to correlate with the OTFT performance, and their electrochemical properties are correlated with the device stability. It will be seen that transistor performance can be understood in terms of the polymer electronic structure, as well as in terms of the polymer film morphology and microstructure.

**Synthesis of Monomers and Polymers.** The key compound dibromo TPD **3** (Scheme 1) was first synthesized by Tour,[57] and a modified procedure was subsequently developed by Bjørnholm.[52] Recently, the commercial availability of thiophene-3,4-dicarboxylic acid makes the synthesis of **3** far more straightforward.[34] Dehydration of the dicarboxylic acid in acetic anhydride affords anhydride **1**, which was purified by recrystallization from toluene. However, one-step imidization for the synthesis of TPD is not successful under conditions typically employed in the synthesis of phthalimide[55] or naphthalene diimide (NDI).[54] Therefore, a two-step procedure was used for the synthesis of imide **2**. After reaction with the appropriate amines in toluene, the anhydride was converted to the corresponding 4-alkylcarbamoylthiophene-3-carboxylic acid, which can be used for the $SOCl_2$-assisted imidization without further purification. Imide **2** was purified by column chromatography, and subsequent bromination affords the key compound class **3**. The synthesis of TPD derivatives **5** with flanking thiophenes was straightforward, subjecting **3** to reaction with the corresponding 2-trimethylstannyl-3-alkylthiophenes[51] under Stille coupling conditions to afford monomer precursors **4**. TPD derivatives **5** were then obtained in good yields (77%−88%) by bromination of **4**. The distannyl comonomers **6** and **7** for Stille coupling were synthesized and purified following published procedures (Supporting Information).[51]

For comparison with BTI-based homopolymers (Figure 1), TPD-based homopolymer **P1** was synthesized via Yamamoto coupling (Scheme 2). The copolymers **P2**−**P8** were synthesized using Pd-catalyzed Stille coupling.[51] The reactions were quenched in methanol, and the product polymers were collected by filtration and purified by Soxhlet extraction. To achieve sufficient solubility/processability (5−10 mg/mL) for OTFT fabrication, we strategically choose appropriate solubilizing side chains. All polymers (structures shown in Scheme 2) achieve sufficient solubility/processability for thin film and OTFT fabrication/characterization. Because of the smaller TPD core versus that of BTI, all TPD-based polymers show enhanced solubility/

**Table 1. Optical and Electrochemical Properties of Polymers P1−P8 versus Those of P3HT**

| polymer | $M_n$ (kDa) / PDI[a] | $\lambda_{max}$ abs sol (nm)[b] | $\lambda_{shoulder}$ abs sol (nm)[b] | $\lambda_{max}$ abs film (nm)[c] | $\lambda_{shoulder}$ abs film (nm)[c] | $E_g^{opt}$ (eV)[d] | $E_{ox}^{onset}$ (V)[e] | $E_{HOMO}$ (eV)[f] | $E_{red}^{onset}$ (V)[e] | $E_{LUMO}$ (eV)[g] |
|---|---|---|---|---|---|---|---|---|---|---|
| **P1** | 4.7/3.80 | 449 | N.A. | 464 | N.A. | 2.15 | N.A. | N.A. | −1.34 | −3.46 |
| **P2** | 4.8/2.17 | 566 | 618, 662 | 640 | 579 | 1.74 | 0.93 | −5.73 | −1.53 | −3.27 |
| **P3a** | 8.7/1.65 | 481 | 589, 641 | 579 | 636 | 1.83 | 0.75 | −5.55 | N.A. | N.A. (−3.72[h]) |
| **P3b** | 7.3/1.67 | 477 | 591, 642 | 579 | 642 | 1.80 | 0.73 | −5.53 | N.A. | N.A. (−3.73[h]) |
| **P3c** | 14.0/1.67 | 596 | 551, 648 | 586 | 641 | 1.79 | 0.74 | −5.54 | N.A. | N.A. (−3.75[h]) |
| **P4** | 7.6/1.73 | 497 | 573, 627 | 577 | 625 | 1.79 | 0.70 | −5.50 | N.A. | N.A. (−3.71[h]) |
| **P5** | 9.4/1.77 | 630 | 506, 578 | 629 | 535, 578 | 1.82 | 0.72 | −5.52 | N.A. | N.A. (−3.70[h]) |
| **P6** | 9.8/1.86 | 545 | 650 | 647 | 590 | 1.76 | 0.67 | −5.47 | N.A. | N.A. (−3.71[h]) |
| **P7a** | 14.1/1.91 | 471 | N.A. | 581 | 530 | 1.83 | 0.61 | −5.41 | N.A. | N.A. (−3.58[h]) |
| **P7b** | 15.7/1.72 | 473 | N.A. | 583 | 540 | 1.82 | 0.62 | −5.42 | N.A. | N.A. (−3.60[h]) |
| **P7c** | 18.0/1.96 | 475 | N.A. | 585 | 535 | 1.82 | 0.60 | −5.40 | N.A. | N.A. (−3.58[h]) |
| **P8** | 8.3/1.75 | 612 | 681 | 626 | 683 | 1.66 | 0.31 | −5.11 | N.A. | N.A. (−3.45[h]) |
| **P3HT** | 33.8/1.26 | 447 | N.A. | 551 | 603 | 1.90 | 0.36 | −5.16 | N.A. | N.A. (−3.26[h]) |

[a] GPC versus polystyrene standards, trichlorobenzene as eluent, measured at 170 °C. [b] Solution absorption spectra ($1 \times 10^{-5}$ M in chloroform). [c] Thin film absorption spectra from pristine film cast from 5 mg/mL chloroform solution. [d] Optical energy gap estimated from absorption edge of the as-cast thin film. [e] Electrochemically determined vs $Fc/Fc^+$. [f] $E_{HOMO} = -(E_{ox}^{onset} + 4.80)$. [g] $E_{LUMO} = -(E_{red}^{onset} + 4.80)$. [h] Values in the parentheses calculated according to: $E_{LUMO} = E_g^{opt} + E_{HOMO}$.

processability over the corresponding BTI-based polymers, therefore permitting use of shorter or less branched side chains, and thus expanding the available library of TPD-based polymers (Figure 1). For example, **P2** with 2-hexyldecyl is highly soluble, while for BTI-based polymers, "swallow-tail"-like side chains (e.g., 1-octylnonyl) must be employed to achieve sufficient solubility.[51] Polymer **P4**, in which the oligothiophene donor contains three thiophene units, two of which are functionalized with linear *n*-tetradecyl chains, could also be synthesized. In marked contrast, the corresponding BTI polymer with identical side chains and oligothiophene donor is highly insoluble. Note that for **P7b** and **P7c**, the solubility is greater than 40 mg/mL in $CHCl_3$ at 25 °C, which is ideal for many printing techniques.[58,59] High-temperature GPC (170 °C, trichlorobenzene) yields $M_n$ = 4.8−18.0 kDa for these copolymers, while the homopolymer has a lower $M_n$ = 4.7 kDa. $^1$H NMR (Supporting Information) and elemental analysis (EA) establish the identity and purity of these new materials. Although the smaller TPD core provides enhanced solubility, due to the additive intermolecular interactions, careful choice of alkyl substituents is required to achieve optimum solubility. Thus, structures analogous to some of the polymers in Scheme 2 but having different solubilizing substituents and limited solubility are depicted in Scheme S1. For example, the **P2** analogue with $R^1$ = 2-butyloctyl has limited solubility for OTFT fabrication. If $R^1$ = *n*-dodecyl in **P5**, the majority of this **P5** analogue is insoluble. When $R^1$ and $R^2$ are changed to *n*-tetradecyl, the new **P5** analogue is still insoluble. Finally, by employing a branched 2-hexyldecyl group, **P5** is highly soluble in chlorinated solvents.

To study the effects of end-capping on OTFT performance and stability, in the synthesis of polymer **P7c**, after polymerization at 110 °C for 72 h, one-half of the reaction mixture was immediately quenched by precipitating in MeOH before adding the end-cap, and the other half was treated with the chain-end-capping thiophene reagents, 2-(tributylstannyl)thiophene and 2-bromothiophene, sequentially. For better comparison, both products were then subjected to the same purification and processing procedures for OTFT fabrication and characterization. X-ray photoelectron spectroscopy (XPS) was used to investigate the difference of ending group between the two samples. Initial XPS investigation was performed on as-cast polymer films (see the Supporting Information for details), but no significant peaks were detected for Br and Sn due to their low concentrations. To increase the concentration of Sn, the deposited polymer films were subjected to calcination at 540 °C, and as expected a significantly more prominent Sn signal was detected for **P7c** without end-capping than for the polymer with end-capping (Figure S35). No signals from Br were detected due to high-temperature calcination, but a higher concentration of Br in **P7c** without end-capping can be expected. On the basis of the XPS data, end-capping significantly reduces the concentration of Sn and Br as end groups, and it is reasonable to propose that the polymer chains are end-capped with thiophene units.

**Polymer Optical Properties.** The optical properties of the TPD-based polymers were investigated by UV−vis absorption spectroscopy in solution and as thin films; relevant data are summarized in Table 1. Figure 2 shows the absorption spectra of **P1**, **P2**, **P3b**, **P4**, **P7b**, and **P8** in chloroform and as thin films. These polymers have incrementally increased oligothiophene unit conjugation lengths from 0 (**P1**) to 4 (**P7b**), and also contain a strong dialkoxybithiophene electron donor (**P8**). Homopolymer **P1** exhibits weak absorption in the visible region; from solution to film state, the absorption maximum ($\lambda_{max}$) is slightly bathochromically shifted by 15 nm from 449 to 464 nm. The $\lambda_{max}$ of **P1** is blue-shifted by 60 nm, and the calculated $E_g^{opt}$ is 0.15 eV larger than that of the corresponding BTI homopolymer.[50] It is interesting to note here that although the DFT calculations[53] and the single-crystal X-ray diffraction structure determination[60] indicate significant coplanarity of the TPD dimer, the large experimental band gap of **P1** clearly indicates a rather limited conjugation length and/or very weak intermolecular interactions. All of the other donor−acceptor copolymers **P2**−**P8** exhibit large oscillator strengths in the visible region, ranging from $\lambda_{max}$ = 577 nm to $\lambda_{max}$ = 647 nm for the thin films, and the calculated $E_g^{opt}$'s for polymers **P2**−**P7** fall within a small range centered around 1.80 eV (Table 1). The comparable band gaps for **P2**−**P7**

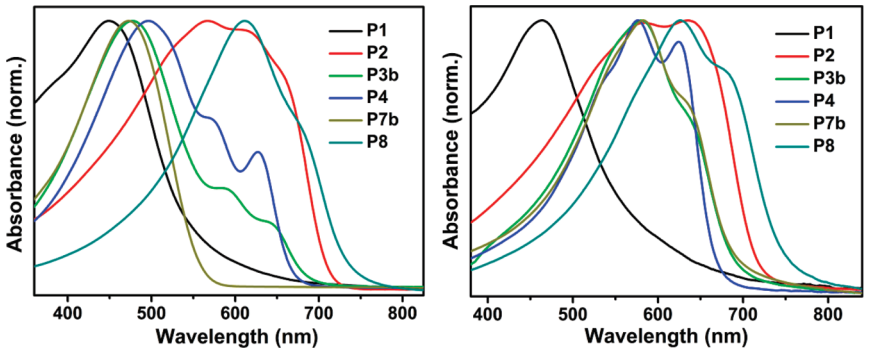


**Figure 2.** Optical absorption spectra of TPD-based homopolymers **P1** and copolymers **P2**, **P3b**, **P4**, **P7b**, and **P8** having varied electron-donating abilities in chloroform (left, $1 \times 10^{-5}$ M) and as pristine films (right) cast from chloroform (5 mg/mL).

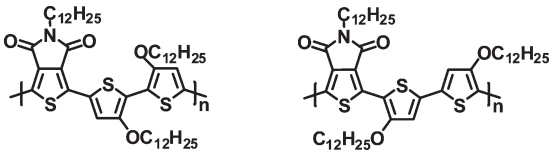


**Figure 3.** Chemical structures of the head-to-head (HH) dialkoxybithiophene containing polymer (left) reported previously[40] and the tail-to-tail (TT) dialkoxybithiophene containing polymer **P8** (right) reported in this work.

can be ascribed to similar backbone conformations and donor−acceptor interactions. The $E_g^{opt}$'s of **P2**−**P7** are about 0.1 eV smaller than that of P3HT,[61,62] which indicates the TPD units depress both the HOMO and the LUMO energies of **P2**−**P7**; however, the LUMO energies are depressed ca. 0.1 eV more than the HOMO levels. The lower-lying HOMOs portend greater OTFT environmental stability than that of P3HT.

The insertion of oxygen atoms between the alkyl substituents and the thiophene core leads to 135 and 47 nm red-shifts in the **P8** $\lambda_{max}$ in comparison to those of **P3b** solutions and thin films, respectively. Furthermore, the $E_g^{opt}$ of **P8** is 0.14 eV smaller than that of **P3b**, doubtless reflecting the stronger electron-donating ability of the dialkoxybithiophene unit in **P8**.[54] The electron-rich character of the dialkoxybithiophene fragment decreases the band gap of **P8**;[63] however, it raises the HOMO energy as evidenced by the CV measurements (vide infra), which will erode OTFT air stability. It is interesting to compare the optical absorption spectrum of **P8** with that of a dialkoxybithiophene-based TPD polymer containing a head-to-head (HH) linkage (structures shown in Figure 3),[40] where both polymers share the same building block but with different arrangements of alkoxy side chains. The HH linkage containing polymers[40] have a 0.16 eV smaller band gap than that of **P8**. DFT computations (Figure S37) indicate that there is a 17 °C angle torsion between the two 3-alkoxythiophene units in the TT linkage, whereas the core is completely planar in the HH linkage due to (thienyl)S···O-(alkoxy) interactions. This leads to greater coplanarity and smaller band gaps for the HH-containing polymers.

The optical absorption features of type **P3** (**P3a** and **P3b**) and **P7** (**P7a**, **P7b**, and **P7c**) polymers are significantly red-shifted (99−110 nm) from the solution to thin film phase (Figure 4), which indicates insignificant aggregation in solution and/or very strong intermolecular interactions in the film state. Variation of solubilizing alkyl substituent dimensions from *n*-decyl to *n*-dodecyl to *n*-tetradecyl does not significantly alter the **P3** and **P7** absorption profiles in either phase. However, **P3c** exhibits a very different absorption profile as compared to **P3a** and **P3b** in chloroform solution. The longer solubilizing side chains (*n*-tetradecyl) apparently do not facilitate the formation of molecularly dissolved **P3c** in chloroform solution, but lead to significantly higher aggregation, with the $\lambda_{max}$ of **P3c** red-shifted by 115 and 119 nm in chloroform versus those of **P3a** and **P3b**, respectively. **P3c** also exhibits greater conjugation and/or greater intermolecular interactions in the film state, as evidenced by a 7 nm red-shift of $\lambda_{max}$ versus those of **P3a** and **P3b**. The tentative explanation for this phenomenon is the greatly extended **P3c** $\pi$-conjugation resulting from the higher $M_n$ and higher degree of side-chain-driven crystallinity versus **P3a** and **P3b**.[64,65] These characteristics are in good agreement with the lower observed solubility of **P3c** versus those of **P3a** and **P3b**, and the greater $\pi$-delocalization and/or stronger intermolecular interactions in **P3c** also explain the far higher OTFT hole mobility (>10×) than in **P3a** and **P3b** (see below). For polymers **P5**, **P6**, and **P7b** containing tetrathiophene donor counits, but having different patterns of solubilizing side-chain substitution, the optical absorption spectra (Supporting Information) reveal that they have varied degrees of aggregation in solution, but similar absorption profiles in the solid state. The thin films of the present TPD-based polymers, except homopolymer **P1**, exhibit both an absorption maximum and an absorption shoulder, similar to the vibronic profiles seen in regioregular polythiophene spectra,[66] and indicating significant polymer chain ordering in the film state.[67]

**Polymer Electrochemical Properties.** The electrochemical properties of all present TPD-based polymers were investigated as thin films using cyclic voltammetry (CV); the ferrocene/ferrocium ($Fc/Fc^+$) redox couple was used as internal standard, and P3HT was measured under the same conditions for comparison. The cyclic voltammograms are shown in Figure 5, and relevant data are collected in Table 1. All electrochemical potentials are reported versus SCE, which has an energy of −4.44 eV below the vacuum level.[68] For some CV traces, the reference $Fc/Fc^+$ redox couple is only partially reversible and/or relatively poorly resolved, which may be due to the thick polymer films preventing penetration of ferrocene and the electrolyte to the electrode. As seen from Figure 5, only homopolymer **P1** and copolymer **P2** having monothiophenes as donors exhibit visible reduction peaks with onsets (vs $Fc/Fc^+$) of −1.34 and −1.53 V, respectively, yielding electrochemically derived LUMO energies of −3.46 and −3.27 eV for **P1** and **P2**, respectively. As the conjugation length of the oligothiophene donor counits is further

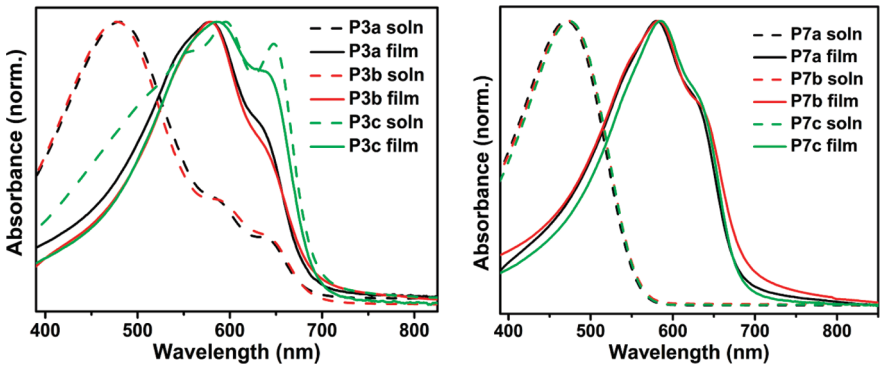


**Figure 4.** Optical absorption spectra of polymers **P3** (left) and **P7** (right) having varied solubilizing substituents in chloroform solution (dashed line, $1 \times 10^{-5}$ M) and as pristine films (solid line) cast from chloroform (5 mg/mL).

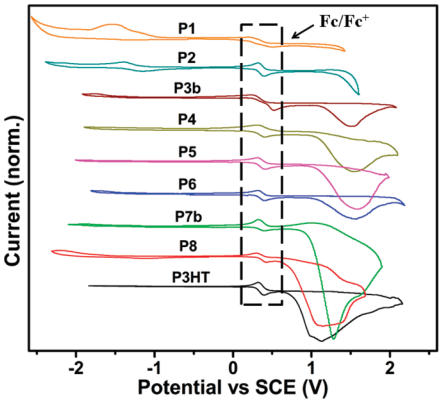


**Figure 5.** Cyclic voltammograms of TPD-based polymer thin films in 0.1 M $(n\text{-Bu})_4N \cdot PF_6$ acetonitrile solution (the $Fc/Fc^+$ redox couple was used as an internal standard having an oxidation potential of +0.36 V vs SCE). P3HT is shown for comparison.

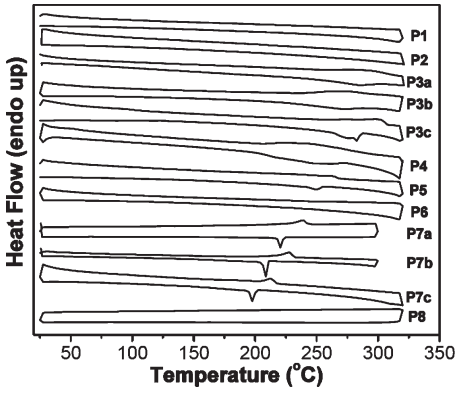


**Figure 6.** DSC thermograms of the indicated TPD-based polymers at a temperature ramp rate of 10 °C/min under $N_2$. The top line is from the heating run, and the bottom line is from the cooling run.

increased, the reduction peaks disappear, and oxidation peaks are evident. Thus, incorporation of electron-donating counits leads to a not unexpected destabilization of the LUMOs. The coexistence of oxidation and reduction processes in **P2** suggests it could operate as an ambipolar material, in good agreement with the OTFT performance (vide infra). On the basis of the oxidation potential onsets, the calculated HOMO energies for the present series are −5.73, −5.53, −5.50, −5.52, −5.47, and −5.42 eV for **P2**, **P3b**, **P4**, **P5**, **P6**, and **P7b**, respectively. The conjugation length extension in oligothiophene series **P3**→**P7** generally leads to decreased ionization potentials (IPs), meaning higher-lying HOMOs, and indicating potentially enhanced p-type OTFT response if all other factors remain constant. As expected, changes in alkyl substituent lengths have negligible influence on the polymer electrochemical properties; for example, **P3a**, **P3b**, and **P3c** exhibit very similar CV responses and comparable HOMO energies (−5.53 to −5.55 eV), as do polymers **P7a**, **P7b**, and **P7c** (−5.40 to −5.42 eV). However, introducing dialkoxybithiophene as the donor counit significantly destabilizes the HOMO of **P8**, resulting in the highest-lying HOMO of the series, −5.11 eV, which lies even higher than that of P3HT by 0.05 eV. It is interesting to compare the HOMO of **P8** with the polymer discussed above having an HH linkage and containing dialkoxybithiophene units (structure shown in Figure 3), which has a ∼0.2 eV higher HOMO than does P3HT.[40] Thus, the tail-to-tail (TT) linkage in **P8** leads to a 0.16 eV larger $E_g^{opt}$, but also a 0.15 eV lower HOMO energy than in the HH linkage containing polymer. On the basis of the HOMOs derived from the CV measurements, polymers **P2**−**P7** should exhibit significantly enhanced p-type OTFT device stability versus P3HT.

**Polymer Thermal Properties.** Thermal analysis of the TPD-based polymers **P1**−**P8** was carried out by differential scanning calorimetry (DSC) at a temperature ramp rate of 10 °C/min. Homopolymer **P1** shows no visible thermal transitions up to 320 °C (Figure 6), which indicates an amorphous structure as expected from the optical properties (see above). The incorporation of a monothiophene unit as the donor counit does not induce a phase transition in copolymer **P2**, which also exhibits a featureless DSC thermogram. Further extension of the donor counits to the TT linkage containing a bithiophene fragment leads to pronounced thermal transitions for the **P3** type polymers. Polymers **P3a** and **P3b** exhibit distinct thermal transitions at 290 °C/284 °C and at 275 °C/271 °C during the heating/cooling cycles, respectively. Except for **P3c**, the polymers functionalized with longer side chains exhibit lower transition temperatures,[2] and the polymers of type **P7** follow the same trend. **P3c** is the only polymer in the series that clearly exhibits two discrete endotherms (276 and 300 °C) on heating and two exotherms (274 and 283 °C) on cooling, similar to that observed in liquid-crystalline PBTTT.[13] The first transition can be ascribed to a solid−mesophase transition, and the second transition can be ascribed to a mesophase−isotropic transition. The first transition temperature couple (276 °C/274 °C) of **P3c** is higher than that

**Table 2. Bottom-Gate/Top-Contact (BG/TC) OTFT Device Performance for TPD-Based Polymers P1−P8 Measured under Ambient Conditions**

| polymer | $T_{annealing}$ (°C) | $\mu$ ($cm^2\ V^{-1}\ s^{-1}$)[b,c] | $V_t$ (V) | $I_{on}/I_{off}$ |
|---|---|---|---|---|
| **P1**[a] | 150 | NA | NA | NA |
| **P2**[a] | 150 | $1.0 \times 10^{-3}$ (e) [$1.1 \times 10^{-3}$] | 30 | 11 |
| | | $2.5 \times 10^{-4}$ (h) [$4.1 \times 10^{-4}$] | −16 | 6 |
| **P3a** | 150 | $4.5 \times 10^{-3}$ (h) [$4.1 \times 10^{-3}$] | −14 | $7 \times 10^3$ |
| **P3b** | 150 | $3.5 \times 10^{-3}$ (h) [$3.7 \times 10^{-3}$] | −22 | $1 \times 10^4$ |
| **P3c** | 210 | 0.175 (h) [0.189] | −12 | $8 \times 10^6$ |
| **P4** | 210 | 0.175 (h) [0.585] | −22 | $5 \times 10^5$ |
| **P5** | 180 | $9.8 \times 10^{-2}$ (h) [0.216] | −18 | $1 \times 10^5$ |
| **P6** | 150 | $3.4 \times 10^{-3}$ (h) [$3.8 \times 10^{-3}$] | −10 | $1 \times 10^3$ |
| **P7a** | 180 | $9.2 \times 10^{-2}$ (h) [0.101] | −11 | $2 \times 10^4$ |
| **P7b** | 210 | 0.136 (h) [0.141] | −17 | $2 \times 10^5$ |
| **P7c** | 150 | 0.104 (h) [0.108] | −24 | $5 \times 10^4$ |
| **P8** | 90 | $4.7 \times 10^{-3}$ (h) [$5.1 \times 10^{-3}$] | −14 | $6 \times 10^2$ |

[a] Measured under vacuum. [b] h and e indicate hole and electron mobilities, respectively. [c] Maximum mobilities are shown in brackets. NA stands for non-active.

of **P3b**, which can be correlated with the higher crystallinity and/or stronger intermolecular interactions, also in good agreement with the optical properties. The insertion of substituent oxygen atoms yields polymer **P8**, which does not exhibit an obvious thermal transition. As the conjugation lengths are increased to terthiophene **P4** and tetrathiophenes **P5**, **P6**, and **P7**, all polymers exhibit pronounced thermal transitions except **P6**. Within the series, all polymers in the **P7** category exhibit sharp thermal transitions. Increasing the solubilizing alkyl substituents by two carbon atoms incrementally depresses the transition temperature from **P7a** (240 °C/220 °C) to **P7b** (228 °C/209 °C) to **P7c** (212 °C/197 °C). As compared to **P7b**, the deletion of two *n*-dodecyl chains from thiophene units adjacent to TPD leads to the disappearance of the thermal transition in **P6**, while deletion of the two *n*-dodecyl chains from thiophene units that are more distant to the TPD units preserves the thermal transition. This polymer structure is shown in Scheme S1 because the material is not sufficiently soluble for OTFT fabrication and is structurally analogous to **P5** with $R^1$ = *n*-dodecyl. Note that polymer **P5** maintains the thermal transition at 261 °C/250 °C during the heating/cooling cycle. Therefore, the alkyl substituents not only provide the good solubility/processability for device fabrication, but can also afford the cohesive forces for crystallinity[69] if they are suitably manipulated. We will see below that these trends in thermal transitions are strongly correlated with the corresponding thin-film microstructures and OTFT device performance. The DSC investigations indicate that the TPD-based polymer semiconductors exhibit greater film crystallinity, and it will be seen that this leads to significantly higher OTFT mobilities versus the corresponding BTI-based polymers (vide infra).[51]

**Field-Effect Transistor Fabrication and Characterization.** Bottom-gate/top-contact (BG/TC) OTFTs were fabricated[51] to investigate the charge transport properties of the present TPD-based polymers. For the BG/TC devices, the polymer semiconductors were deposited by spin-coating 10 mg/mL chloroform solutions in ambient onto hexamethyldisilazane (HMDS)-modified, p-doped Si (001) wafers having a 300 nm thermally grown $SiO_2$ dielectric layer (see the Supporting Information for details). The capacitance of the $SiO_2$ gate insulator is ~12 nF $cm^{-2}$. After spin-coating, the polymer films were annealed at selected temperatures under $N_2$ or vacuum for 1 h, and Au electrode deposition completed the device fabrication (channel length = 50 or 100 $\mu$m, channel width = 5000 $\mu$m). Devices were typically characterized under ambient conditions except for those of **P1** and **P2**. Mobilities were calculated from saturation regimes, and the average data (at least five devices were measured for each sample) are collected in Table 2 together with current modulation ($I_{on}/I_{off}$ ratios) and threshold voltages ($V_t$'s) for the present TPD polymers (maximum mobilities are shown in brackets). Figure 7 shows characteristic transfer and output plots of transistors fabricated from polymers **P3c**, **P4**, and **P7b**, which showed the best electrical performance under optimized fabrication conditions.

In contrast to our previously reported n-type BTI-based homopolymer (structure shown in Figure 1),[50,51] TPD-based homopolymer **P1** is TFT-inactive under the conditions used for OTFT fabrication and characterization, which may be due to the unfavorable frontier molecular orbital (FMO) energies and a large band gap, as discussed above. This large gap is consistent with limited conjugation due to the decreased molecular coplanarity and/or limited intermolecular interactions.[70] Also consistent with the lack of TFT activity is the poor crystallinity evident in the DSC data (Figure 6). In contrast, when a monothiophene is included as a donor counit, copolymer **P2** achieves effective conjugation via reduced steric hindrance and exhibits ambipolar OTFT behavior under vacuum, with electron and hole mobilities of $1.0 \times 10^{-3}$ and $2.5 \times 10^{-4}$ $cm^2\ V^{-1}\ s^{-1}$, respectively. The ambipolarity of **P2**-based OTFTs is in good agreement with the electrochemical properties, showing both oxidative and reductive events in the cyclic voltammetry (Figure 5). These moderate mobilities can be ascribed to the substantial energetic barrier between the electrode Fermi level and the semiconductor FMO energy levels, which inhibits charge injection,[71] and to the low crystallinity revealed by the DSC data (Figure 6), which erodes efficient charge transport. As expected, further increasing the conjugation length of oligothiophene counits in polymers **P3**−**P7** or enhancing the electron donating ability of the donor counit in **P8** results in enhanced p-type response in the OTFTs. The polymers showing the best performance among the series are **P3c** and **P4**, with an average hole mobility of 0.175 $cm^2\ V^{-1}\ s^{-1}$. Note that a very high maximum mobility of 0.585 $cm^2\ V^{-1}\ s^{-1}$ is observed for **P4**-based OTFTs after 210 °C thermal annealing, with **P3** having a bithiophene donor counit and **P4** a terthiophene one. Note that **P5** and **P7** exhibit slightly lower average hole mobilities (~0.1 $cm^2\ V^{-1}\ s^{-1}$) in OTFTs, both having tetrathiophene as donor counits. The substantial mobilities (>$10^{-3}$ $cm^2\ V^{-1}\ s^{-1}$) of the **P3**−**P8**-based OTFTs indicate favorable hole injection from the contacting electrodes to the HOMOs. The HOMOs of **P3c** and **P4** are lower than those of **P5**−**P8**, indicating greater barriers for charge injection; therefore, the superior hole mobilities must correlate with their optimal film microstructures and morphologies (vide infra). The modification of the alkyl side-chain substituent lengths does not significantly impact the device performance of the type **P7** polymers, and **P7a**, **P7b**, and **P7c** exhibit comparable OTFT performance with $\mu_h$ = 0.092, 0.136, and 0.104 $cm^2\ V^{-1}\ s^{-1}$, respectively (Table 2), indicating similar charge injection and transport. For polymers of type **P3**, **P3c** shows more than 10× greater hole mobility than do **P3a** and **P3b** due to the substantial conjugation as revealed by optical absorption and by

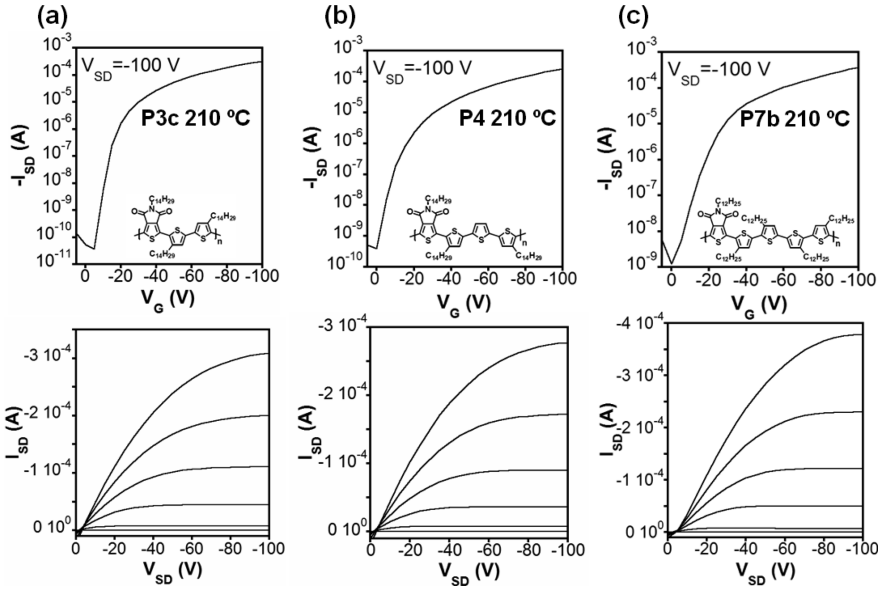


**Figure 7.** Transfer (top) and output (bottom) characteristics for (a) **P3c**-, (b) **P4**-, and (c) **P7b**-based BG/TC OTFTs annealed at 210 °C. In the output plots, the gate voltage varies from 20 to −100 V (channel width: 5000 $\mu$m; channel lengths: 100, 100, and 50 $\mu$m for **P3c**, **P4**, and **P7b**, respectively).

the crystallinity evident in the DSC data (Figure 6). **P7b** was chosen to fabricate top-gate/bottom-contact (TG/BC) devices (see the Supporting Information for fabrication details). TG/BC OTFTs were fabricated on glass substrates having Au source-drain contacts, a spin-coated semiconductor film, a spin-coated dielectric film, and a thermally evaporated top Al gate. These OTFTs exhibit an average $\mu_h = 0.24 \pm 0.025$ cm$^2$ V$^{-1}$ s$^{-1}$, $I_{on}/I_{off} = 10^3-10^4$, and $V_t = -15$ V (Figure S40). These results are very promising for printed devices considering the high solubility of **P7b** (>40 mg/mL at room temperature).

It is instructive to compare the $I_{on}/I_{off}$ ratios (Table 2) and the off-currents (Figure 7) for the **P3c**, **P4**, and **P7b**-based OTFTs. Note that the increased conjugation length from bithiophene to terthiophene to tetrathiophene leads to decreased $I_{on}/I_{off}$ ratios and increased off-currents, which correlates with the progressive HOMO rise from −5.54 eV (**P3c**) to −5.50 eV (**P4**) to −5.42 eV (**P7b**). The $I_{on}/I_{off}$ ratio of the **P8**-based device is $6 \times 10^2$, the lowest for OTFTs fabricated from the **P3**−**P8** series, and readily ascribable to its highest-lying HOMO (−5.11 eV). Therefore, extension of the oligothiophene $\pi$-systems in the donor comonomers and/or introducing the electron-rich dialkoxybithiophene unit destabilizes the polymer HOMOs, leading to a high p-doping tendency of the materials in the off-state.

Recently, Heeger studied chain end-capping effects on polymer solar cell performance and reported that end-capping the active layer polymer backbone with thiophene units improves device performance by making the solar cell performance less sensitive to the active layer thickness and to thermal degradation, but without significant changes in power conversion efficiency (~10%).[72] For polymer **P7c**, we chose the same batch for the study of the end-capping effects on OTFT performance, one sample with thiophene end-capping and one without. Although XPS indicates significant differences in Sn concentration (Figure S35) between the two samples, no substantial differences (<10%) in OTFT performance were observed in either hole mobility or $I_{on}/I_{off}$ ratio. After annealing at 180 °C, OTFTs fabricated from **P7c** with end-capping show an average $\mu_h = 0.071$ cm$^2$ V$^{-1}$ s$^{-1}$ and $I_{on}/I_{off} = 2 \times 10^5$, while OTFTs fabricated from **P7c** without end-cap show an average $\mu_h = 0.072$ cm$^2$ V$^{-1}$ s$^{-1}$ and $I_{on}/I_{off} = 2 \times 10^5$. Similar results are found for **P7c** OTFTs annealed at other temperatures.

**Polymer Film Microstructure and Morphology. Correlation with Carrier Transport.** Optimum film microstructures and morphologies are critical for charge transport in organic transistors, and specular X-ray diffraction (XRD) and tapping mode atomic force microscopy (AFM) were employed to investigate the structural ordering of the present TPD-based polymer films. Analysis of the film microstructures and morphologies provides valuable information on the effects of two different structural modifications, $\pi$-core expansion of oligothiophene donor counits and modification of length or positional pattern of the alkyl side chains, as well as film processing conditions, for example, annealing temperature, in the TPD-based polymers. It will be seen that the film structural orderings correlate well with OTFT device performance.

Figure 8 shows Θ−2Θ XRD scans for **P1**−**P8** films under the conditions yielding optimum BG/TC OTFT performance. A single family of Bragg reflections is found for all of the polymers. The XRD scans of **P1** and **P2** films show relatively low crystallinity with maximum reflections up to second order, accompanied by low intensities. The AFM images also show featureless textures (Figure S41). The low crystalline microstructures of **P1** and **P2**, together with their unfavorable FMO energies, result in TFT inactivity and low TFT carrier mobilities ($\mu_e$: $10^{-3}$ cm$^2$ V$^{-1}$ s$^{-1}$; $\mu_h$: $10^{-4}$ cm$^2$ V$^{-1}$ s$^{-1}$) for **P1** and **P2**, respectively. Further expansion of the oligothiophene donor counit $\pi$-core to bithiophene (**P3c**), to terthiophene (**P4**), and to tetrathiophene (**P5** and **P7**) leads to more crystalline film microstructures. In fact, for **P3c**, **P4**, **P5**, **P7a**, **P7b**, and **P7c** films annealed at 210, 210, 180, 180, 210, and 150 °C, respectively, the XRD scans reveal single families of Bragg reflections (Figures 8 and S41), with progressions up to the third or fourth order, indicating highly ordered film microstructures. The film structural orderings result in substantial OTFT hole mobilities for these materials (0.092−0.175 cm$^2$ V$^{-1}$ s$^{-1}$). Finally, in polymer **P8**,

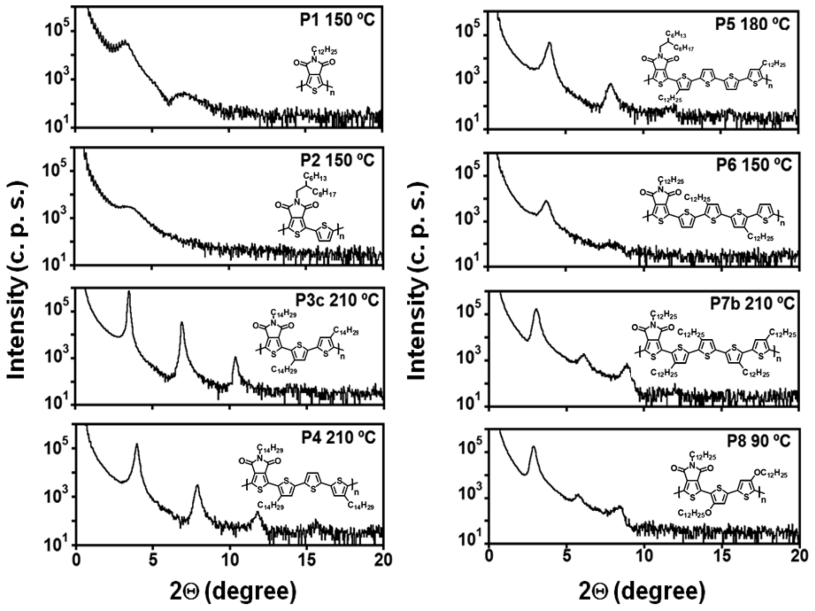


**Figure 8.** XRD scattering patterns of the indicated polymer films annealed at the temperatures resulting in optimum OTFT performance.

the alkyl chains of the bithiophene counits are replaced by alkoxy chains. As judged from the XRD data, this modification leads to greater film crystallinity (Figure 8; with third order Bragg reflections) than in the **P3b** films, where only a weak first order reflection is clearly distinguishable (Figure S42), and results in far more textured morphology as revealed by AFM (Figure S41). In contrast to the XRD data, the DSC scan of **P8** is featureless, while **P3b** exhibits a pronounced thermal transition (Figure 6), and the mobility is enhanced slightly from $3.5 \times 10^{-3}$ to $4.7 \times 10^{-3}$ $cm^2$ $V^{-1}$ $s^{-1}$. Therefore, expansion of oligothiopehene conjugation length generally increases the film crystallinity,[73] in all likelihood a result of the more ordered $\pi-\pi$ stacking of the polymer chains.[23]

For the polymers of type **P3**, *d*-spacings are estimated to be 25.54, 28.41, and 31.00 Å for **P3a**, **P3b**, and **P3c**, respectively, after the films are annealed at selected temperatures (Table S2). The increasing alkyl chain lengths lead to gradually expanded *d*-spacings (lamellar spacings). It was found that longer alkyl chains can in essence self-assemble to afford higher film crystallinity, evident in the XRD diffraction data (Figure S42). For polymers **P3a** and **P3b**, only first-order Bragg reflections were detected in XRD measurements, while **P3c** exhibits reflections up to third order after the films are annealed at the optimal temperatures. The improved film crystallinities are associated with significantly enhanced OTFT electrical performance, and $\mu_h$ increases from $3.5 \times 10^{-3}$ to 0.175 $cm^2$ $V^{-1}$ $s^{-1}$. The greater crystallinity of **P3c** film is also in good agreement with the optical absorption spectra (Figure 4) and DSC measurements (Figure 6), as discussed above. For polymers of type **P7**, increasing lengths of the alkyl chains also leads to greater *d*-spacings, for example, 25.10 Å for **P7a**, 28.97 Å for **P7b**, and 32.24 Å for **P7c** (Table S2). However, modification of the alkyl side-chain length has far less effect on the film morphologies and crystallinities (Figure S43), with **P7a**, **P7b**, and **P7c** all showing Bragg reflections up to third order. Note that the **P7b** films exhibit the greatest relative crystallinity as evidenced by the diffraction intensities, and these results are in good agreement with the device performance of **P7b**-based OTFTs, which exhibit a relatively high average $\mu_h$ = 0.136 $cm^2$ $V^{-1}$ $s^{-1}$ after annealing at 210 °C. This result is closely followed by those for **P7c** and **P7a**-based OTFTs, which have average $\mu_h$ values of 0.104 and $9.2 \times 10^{-2}$ $cm^2$ $V^{-1}$ $s^{-1}$, respectively. Another alkyl side chain modification is the change of the position pattern. Polymers **P5**, **P6**, and **P7b** have tetrathiophene as donor counits. In comparison to **P7b**, two *n*-dodecyl substituents are deleted from the two middle thiophenes in the tetrathiophene counits of **P6**. This modification results in a greatly reduced *d*-spacing from 28.97 Å (**P7b**) to 23.56 Å (**P6**), but leads to significantly lower film crystallinity, with only first-order Bragg reflections detectable in **P6** films, in marked contrast to the third-order reflections of **P7b** films (Figure 8). These crystallinity differences are also in good agreement with the DSC experiments in which no thermal transition is detected for polymer **P6** (Figure 6). The OTFTs fabricated from **P6** show more than 10× lower mobility, with an average $\mu_h = 3.4 \times 10^{-3}$ $cm^2$ $V^{-1}$ $s^{-1}$, as compared to the mobility of **P7b**-based OTFTs, with an average $\mu_h$ = 0.136 $cm^2$ $V^{-1}$ $s^{-1}$. The long chain alkyl substituents apparently not only increase the solubility of polymer **P7b**, but also induce greater film crystallinity. In polymer **P5**, two alkyl chains are also deleted, but from the outer two thiophenes in the tetrathiophene counits. The XRD investigations indicate that **P5** maintains a highly ordered film microstructure with single families of Bragg reflections and progressions up to the fourth order evident (Figure 8). **P5**-based OTFTs exhibit an average $\mu_h$ = 0.098 $cm^2$ $V^{-1}$ $s^{-1}$, comparable to that of **P7b**-based OTFTs. As compared to **P6**, the substantially greater crystallinity of the **P5** films is likely due to a greater degree of side chain interdigitation, enabled by larger local free-volume between the alkyl chains. The film crystallinities are in good agreement with the observed solubility characteristics. While **P6** is highly soluble when the alkyl substituent on the imide nitrogen is *n*-dodecyl, the **P5** analogue is highly insoluble (structure shown in Scheme S1). In contrast, when the substituent is branched 2-hexyldecyl, **P5** achieves substantial solubility for OTFT fabrication. These results clearly indicate the importance of the alkyl substituent position pattern for enhancing film crystallinity in these TPD-based polymers.

Note that the effects of annealing are substantial for polymer **P3c**, where the mobility is dramatically increased from $2.9 \times 10^{-2}$

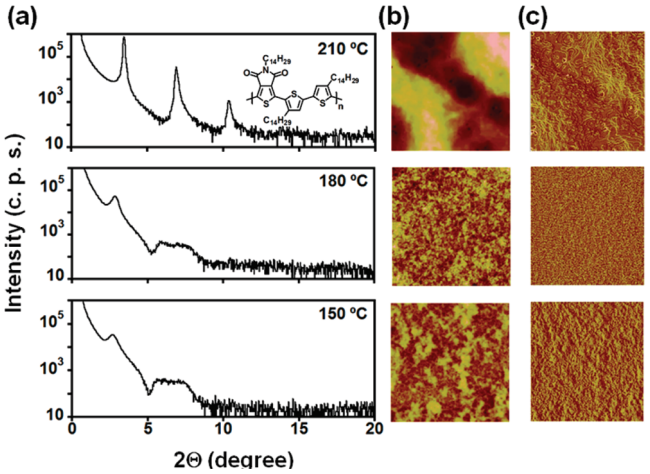


**Figure 9.** (a) XRD scattering patterns of **P3c** films annealed at the indicated temperatures. AFM (5 $\mu$m × 5 $\mu$m) data: (b) topograph images and (c) phase images of the corresponding films.

**Table 3. Changes in the Bottom-Gate/Top-Contact (BG/TC) OTFT Device Performance (Hole Mobilities, $I_{on}/I_{off}$ Ratios, and Threshold Voltages) of Polymers P3c, P4, P5, and P7 on Storage in Air**[a]

| | | initial | | | after storage | | |
|---|---|---|---|---|---|---|---|
| polymer | days | $\mu$ ($cm^2\ V^{-1}\ s^{-1}$) | $I_{on}/I_{off}$ | $V_t$ (V) | $\mu$ ($cm^2\ V^{-1}\ s^{-1}$) | $I_{on}/I_{off}$ | $V_t$ (V) |
| **P3c** | 60 | 0.175 | $8 \times 10^6$ | −12 | 0.161 | $3 \times 10^6$ | −11 |
| **P4** | 60 | 0.175 | $5 \times 10^5$ | −22 | 0.154 | $3 \times 10^5$ | −17 |
| **P5** | 60 | 0.098 | $1 \times 10^5$ | −18 | 0.092 | $8 \times 10^4$ | −15 |
| **P7a** | 118 | 0.092 | $2 \times 10^4$ | −11 | 0.076 | $8 \times 10^2$ | 2 |
| **P7b** | 153 | 0.136 | $2 \times 10^5$ | −17 | 0.132 | $2 \times 10^5$ | −21 |
| **P7c** | 108 | 0.104 | $5 \times 10^4$ | −24 | 0.102 | $2 \times 10^4$ | −18 |

[a] Average values are shown.

to 0.175 $cm^2\ V^{-1}\ s^{-1}$ upon increasing the annealing temperature from 150 to 210 °C (Table S1). This effect is again easily tracked by AFM and XRD characterization (Figure 9), where it can be clearly observed that the crystallinity is greatly enhanced on 210 °C annealing, and the formation of large, terrace-like, crystalline grains is evident in the AFM image versus smaller, less well-defined grains at lower temperatures (Figure 9). These grains are easily distinguishable in the phase image. That the increased grain sizes lead to higher mobilities likely reflects the fact that charge carrier transport across grain boundaries is not as efficient as within ordered domains.[74] Thermal annealing at higher temperatures should result in even higher degrees of alkyl chain interdigitation if the chains have the same tilt angle with respect to the polymer backbones, and indeed the *d*-spacing is gradually decreased from 32.72 Å (150 °C) to 31.00 Å (180 °C) to 25.46 Å (210 °C) (Table S2). In the case of **P4**, the increased mobility with increasing annealing temperature is also observed, but it is less dramatic.

**OTFT Device Stability.** Although the carrier mobilities of polymer-based OTFTs have increased dramatically over the past decade[49,75] and OTFTs have moved toward to commercialization,[17] device environmental stability (or storage lifetime) as well as operational (or bias) stability has come under intense scrutiny.[20] Device storage stability primarily reflects FMO energies.[1,22,71] For polymers **P3c**, **P4**, **P5**, **P7a**, **P7b**, and **P7c** exhibiting hole mobilities approaching or surpassing 0.1 $cm^2\ V^{-1}\ s^{-1}$, OTFT environmental stability was monitored over the course of storage under ambient, and relevant data are collected in Table 3. The temporal evolution of OTFT performance (hole mobility and $I_{on}/I_{off}$) of **P7b** under ambient is plotted in Figure 10. All of the polymer OTFTs evidence robust storage stability from at least 60 days up to more than 5 months of storage under ambient with nearly invariant carrier mobilities, $I_{on}/I_{off}$ ratios, and threshold voltages except for **P7a**. The enhanced ambient storage stability doubtless reflects the low-lying HOMOs created by the electron-deficient TPD units. After 4 months storage in ambient, **P7a**-based OTFTs evidence decreased hole mobility (Table 3), a more than 10× decreased $I_{on}/I_{off}$ ratio, and a substantial shift of the threshold voltage. As compared to **P7a**, both **P7b** and **P7c** have longer aliphatic side chains, which can better screen the polymer backbone from $O_2$ and $H_2O$.[8] For end-capping effects on the OTFT stability, the performance in ambient of **P7c**-based OTFTs both with and without end-capping was monitored, and both show negligible device degradation after more than 2 months.

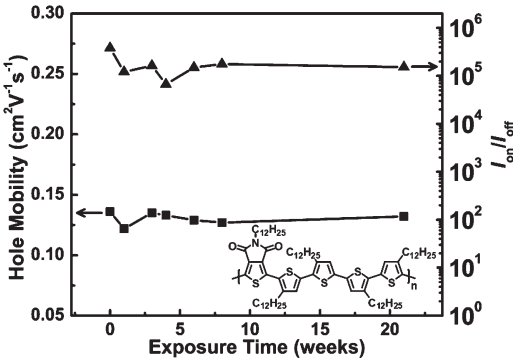


**Figure 10.** Temporal evolution of OTFT performance (hole mobility and $I_{on}/I_{off}$ ratio) for polymer **P7b** devices in air. Average values are shown. The lines are drawn as guides to the eye.

Although OTFTs with impressive storage stability have recently been achieved in new generations of high-performance polymer semiconductors,[2,15,24,76] operational stability is a major challenge faced by OTFTs as well as by other TFT technologies, such as amorphous silicon, polycrystalline silicon, and metal oxide semiconductors.[20,77] Therefore, the operational stabilities of polymer **P3c**-, **P4**-, and **P7b**-based OTFTs fabricated with varied oligothiophene conjugation lengths were evaluated by repeatedly switching the transistors on/off in ambient between $V_G$ = 10 V and $V_G$ = −50 V at fixed $V_{DS}$ = −50 V.[46] All of the present polymer OTFTs show good stability after 1000 on−off cycles (top of Figure 11). The transfer characteristics of the same pixel before and after bias-stress were collected and overlapped (bottom of Figure 11). Among these materials, **P3c** shows the greatest bias stability after cycling, with negligible changes in the transfer characteristics; the hole mobility, $I_{on}/I_{off}$, and threshold voltage remain almost unchanged (before cycling, $\mu_h$ = 0.170 $cm^2\ V^{-1}\ s^{-1}$, $I_{on}/I_{off} = 8.6 \times 10^6$, $V_t$ = −13 V; after cycling, $\mu_h$ = 0.168 $cm^2\ V^{-1}\ s^{-1}$, $I_{on}/I_{off} = 5.0 \times 10^6$, $V_t$ = −12 V). Under the same bias-stress, the on-current of the **P4**-based OTFTs remains unchanged, the off-current is increased by 5× and is accompanied by shift of $V_t$ from −18 to −5 V, and $\mu_h$ is decreased by 20%. For the **P7b**-based OTFTs, the off-current remains unchanged, the on-current is decreased by ∼40% accompanied by slightly shifted $V_t$, and $\mu_h$ falls by 43%. After 1000 on−off cycles, the **P3c**-based OTFT was subjected to

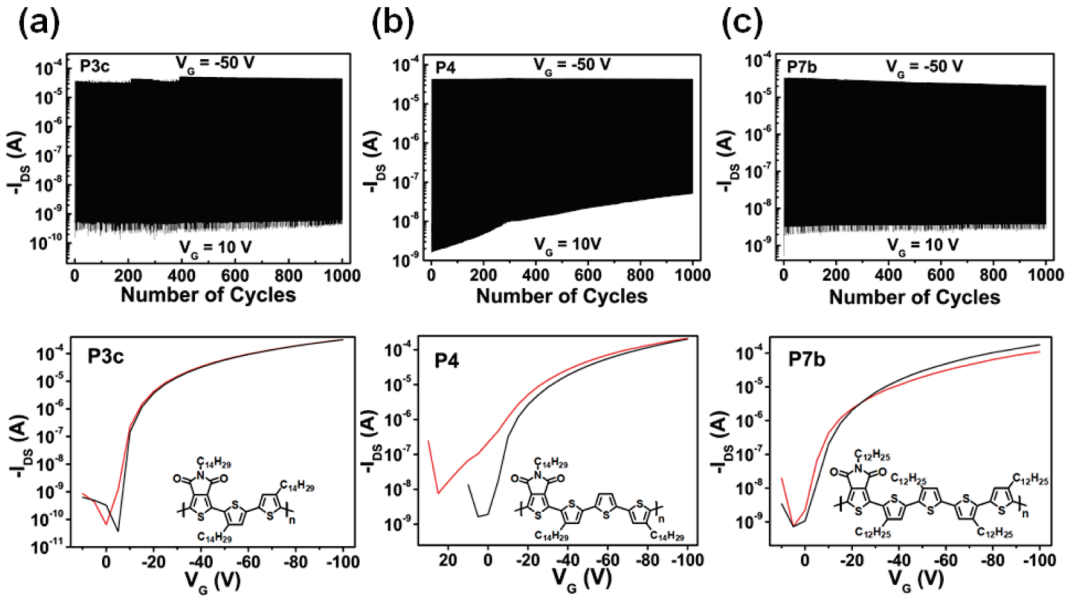


**Figure 11.** On−off cycles at $V_{DS}$ = −50 V (top) under ambient conditions for OTFTs annealed at optimized temperatures, fabricated with polymers **P3c** (a), **P4** (b), and **P7b** (c) and measured at the indicated gate bias. Overlapping of transfer characteristics (bottom) before (black) and after (red) 1000 on−off cycles.

another 1000 cycles under greater bias-stress; between $V_G$ = +10 V and $V_G$ = −70 V with $V_{DS}$ = −70 V, the device exhibits slightly eroded performance (Figure S44). The superior operational stability of the **P3c**-based OTFTs can be ascribed to having the lowest-lying HOMO level of the series, which can better suppress the accumulation of trapped charge at the semiconductor/dielectric interface. We believe the operational stability of **P3c**-based OTFTs can be further improved by engineering the device architecture[77] and gate dielectric.[10,78,79]

## CONCLUSIONS

By incorporating electron-deficient TPD units, we have synthesized a new series of TPD-based polymer semiconductors **P1**−**P8** with varied oligothiophene donor counit conjugation length and solubilizing side chains for OTFT applications. The alkyl substituent position provided by the TPD imide unit affords excellent solubilities, as high as 40 mg/mL for **P7b** and **P7c** at room temperature. Homopolymer **P1** has limited $\pi$-conjugation and an amorphous film microstructure and is therefore TFT-inactive, while TPD-based copolymers **P2**−**P8** achieve enhanced $\pi$-conjugation by eliminating imide−imide repulsion. By incorporating monothiophene as a donor counit, **P2** exhibits ambipolar behavior under vacuum with electron and hole mobilities of $\sim 10^{-4}$−$10^{-3}$ cm$^2$ V$^{-1}$ s$^{-1}$. TPD polymers based on bithiophene, terthiophene, and tetrathiophene donor counits (**P3**−**P7**) are p-type semiconductors with hole mobilities approaching or surpassing 0.1 cm$^2$ V$^{-1}$ s$^{-1}$. Among these, the highest hole mobility of ∼0.6 cm$^2$ V$^{-1}$ s$^{-1}$ is observed for OTFTs fabricated from **P4**. The alkyl chains not only enhance solubility, but also significantly promote polymer thin film crystallinity and microstructure as revealed by XRD and AFM measurements. In comparison to **P7**, the absence of alkyl chain substituents on the neighboring thiophenes of TPD leads to decreased film crystallinity in **P6**, and hence to more than 10× lower OTFT hole mobility. The optical properties and device performance of polymers **P7** are basically insensitive to the length of the solubilizing chains. However, in polymers of type **P3**, **P3c** shows distinct red-shifted optical absorption maxima, higher film crystallinity, and enhanced OTFT performance with an average hole mobility of ∼0.2 cm$^2$ V$^{-1}$ s$^{-1}$. The incorporation of electron-rich dialkoxybithiophene units leads to the lowest band gap in the series, but also destabilizes the HOMO in **P8**. For the high-performance semiconductors (mobility >0.1 cm$^2$ V$^{-1}$ s$^{-1}$), both device environmental stability under storage and operational stability under bias were investigated. Because of the low-lying HOMOs, all OTFTs fabricated from **P3c**, **P4**, **P5**, **P7b**, and **P7c** show negligible performance degradation for up to 5 months storage under ambient conditions. Under bias, **P3c** OTFTs are stable with negligible on-current and off-current shifts after 1000 on−off cycles; however, **P4** and **P7b**-based OTFTs show somewhat greater performance degradation when measured in the same bias window. The superior stability of **P3c**-based OTFTs is likely due to the deeper HOMO, which is less sensitive to charge trapping. Because of the ready materials accessibility, excellent solubility/processability, substantial hole mobilities, and good OTFT bias-stability, TPD-based polymers are promising semiconducting materials for high-performance thin-film transistor applications.

## ASSOCIATED CONTENT

**Supporting Information.** Monomer/polymer synthesis and characterization, $^1$H and $^{13}$C NMR spectra, XPS spectra, UV−vis spectra, DFT calculations, DSC trace, OTFT fabrication details, OTFT device data, and thin-film characterization (XRD and AFM) for different polymer deposition conditions, bias−stress data of OTFTs, and complete ref 1. This material is available free of charge via the Internet at http://pubs.acs.org.

## AUTHOR INFORMATION

**Corresponding Author**
a-facchetti@northwestern.edu; t-marks@northwestern.edu

## ■ ACKNOWLEDGMENT

We thank ONR (N00014-05-1-0766), AFOSR (FA9550-08-1-0331), and Polyera Corp. for support of this research, and the NSF-MRSEC program through the Northwestern University Materials Research Science and Engineering Center for characterization facilities (DMR-0520513). R.P.O. acknowledges funding from the European Community's Seventh Framework Programme through a Marie Curie International Outgoing Fellowship (Grant Agreement 234808).

## ■ REFERENCES

(1) McCulloch, I.; et al. *Adv. Mater.* **2009**, *21*, 1091.
(2) Osaka, I.; Zhang, R.; Sauve, G.; Smilgies, D. M.; Kowalewski, T.; McCullough, R. D. *J. Am. Chem. Soc.* **2009**, *131*, 2521.
(3) Osaka, I.; Abe, T.; Shinamura, S.; Miyazaki, E.; Takimiya, K. *J. Am. Chem. Soc.* **2010**, *132*, 5000.
(4) Zhang, W.; Smith, J.; Watkins, S. E.; Gysel, R.; McGehee, M.; Salleo, A.; Kirkpatrick, J.; Ashraf, S.; Anthopoulos, T.; Heeney, M.; McCulloch, I. *J. Am. Chem. Soc.* **2010**, *132*, 11437.
(5) Li, Y.; Singh, S. P.; Sonar, P. *Adv. Mater.* **2010**, *22*, 4862.
(6) Li, Y.; Sonar, P.; Singh, S. P.; Soh, M. S.; van Meurs, M.; Tan, J. *J. Am. Chem. Soc.* **2011**, *133*, 2198.
(7) Bronstein, H.; Chen, Z.; Ashraf, R. S.; Zhang, W.; Du, J.; Durrant, J. R.; Tuladhar, P. S.; Song, K.; Watkins, S. E.; Geerts, Y.; Wienk, M. M.; Janssen, R. A. J.; Anthopoulos, T.; Sirringhaus, H.; Heeney, M.; McCulloch, I. *J. Am. Chem. Soc.* **2011**, *133*, 3272.
(8) Osaka, I.; Abe, T.; Shinamura, S.; Takimiya, K. *J. Am. Chem. Soc.* **2011**, *133*, 6852.
(9) Tsao, H. N.; Cho, D.; Andreasen, J. W.; Rouhanipour, A.; Breiby, D. W.; Pisula, W.; Müllen, K. *Adv. Mater.* **2009**, *21*, 209.
(10) Cho, J. H.; Lee, J.; Xia, Y.; Kim, B.; He, Y.; Renn, M. J.; Lodge, T. P.; Frisbie, C. D. *Nat. Mater.* **2008**, *7*, 900.
(11) (a) Yan, H.; Chen, Z.; Zheng, Y.; Newman, C.; Quinn, J. R.; Dötz, F.; Kastler, M.; Facchetti, A. *Nature* **2009**, *457*, 679. (b) Steyrleuthner, R.; Schubert, M.; Jaiser, F.; Blakesley, J. C.; Chen, Z.; Facchetti, A.; Neher, D. *Adv. Mater.* **2010**, *22*, 2799. (c) Rivnay, J.; Toney, M. F.; Zhang, Y.; Kauvar, I. V.; Wagner, V.; Facchetti., A.; Salleo, A. *Adv. Mater.* **2010**, *22*, 4359.
(12) Tsao, H. N.; Müllen, K. *Chem. Soc. Rev.* **2010**, *39*, 2372.
(13) McCulloch, I.; Heeney, M.; Bailey, C.; Genevicius, K.; MacDonald, I.; Shkunov, M.; Sparrowe, D.; Tierney, S.; Wagner, R.; Zhang, W.; Chabinyc, M. L.; Kline, R. J.; McGehee, M. D.; Toney, M. F. *Nat. Mater.* **2006**, *5*, 328.
(14) Tsao, H. N.; Cho, D. M.; Park, I.; Hansen, M. R.; Mavrinskiy, A.; Yoon, D. Y.; Graf, R.; Pisula, W.; Spiess, H. W.; Müllen, K. *J. Am. Chem. Soc.* **2011**, *133*, 2605.
(15) Lei, T.; Cao, Y.; Fan, Y.; Liu, C.-J.; Yuan, S.-C.; Pei, J. *J. Am. Chem. Soc.* **2011**, *33*, 6099.
(16) (a) Marks, T. J. *MRS Bull.* **2010**, *35*, 1018. (b) Facchetti, A. *Mater. Today* **2007**, *10*, 28.
(17) Arias, A. C.; MacKenzie, J. D.; McCulloch, I.; Rivnay, J.; Salleo, A. *Chem. Rev.* **2010**, *110*, 3.
(18) Sekitani, T.; Zschieschang, U.; Klauk, H.; Someya, T. *Nat. Mater.* **2010**, *9*, 1015.
(19) Klauk, H. *Chem. Soc. Rev.* **2010**, *39*, 2643.
(20) Sirringhaus, H. *Adv. Mater.* **2009**, *21*, 3859.
(21) Osaka, I.; Sauve, G.; Zhang, R.; Kowalewski, T.; McCullough, R. D. *Adv. Mater.* **2007**, *19*, 4160.
(22) Kim, D. H.; Lee, B. L.; Moon, H.; Kang, H. M.; Jeong, E. J.; Park, J. I.; Han, K. M.; Lee, S.; Yoo, B. W.; Koo, B. W.; Kim, J. Y.; Lee, W. H.; Cho, K.; Becerril, H. A.; Bao, Z. *J. Am. Chem. Soc.* **2009**, *131*, 6124.
(23) Osaka, I.; Zhang, R.; Liu, J. Y.; Smilgies, D. M.; Kowalewski, T.; McCullough, R. D. *Chem. Mater.* **2010**, *22*, 4191.
(24) Osaka, I.; Takimiya, K.; McCullough, R. D. *Adv. Mater.* **2010**, *22*, 4993.
(25) Lim, B.; Baeg, K. J.; Jeong, H. G.; Jo, J.; Kim, H.; Park, J. W.; Noh, Y. Y.; Vak, D.; Park, J. H.; Park, J. W.; Kim, D. Y. *Adv. Mater.* **2009**, *21*, 2808.
(26) Chabinyc, M. L.; Endicott, F.; Vogt, B. D.; DeLongchamp, D. M.; Lin, E. K.; Wu, Y.; Liu, P.; Ong, B. S. *Appl. Phys. Lett.* **2006**, *88*, 113514.
(27) Fong, H. H.; Pozdin, V. A.; Amassian, A.; Malliaras, G. G.; Smilgies, D.-M.; He, M.; Gasper, S.; Zhang, F.; Sorensen, M. *J. Am. Chem. Soc.* **2008**, *130*, 13202.
(28) Liu, J.; Zhang, R.; Sauve, G.; Kowalewski, T.; McCullough, R. D. *J. Am. Chem. Soc.* **2008**, *130*, 13167.
(29) Nelson, T. L.; Young, T. M.; Liu, J.; Mishra, S. P.; Belot, J. A.; Balliet, C. L.; Javier, A. E.; Kowalewski, T.; McCullough, R. D. *Adv. Mater.* **2010**, *22*, 4617.
(30) Steudel, S.; Myny, K.; Arkhipov, V.; Deibel, C.; De Vusser, S.; Genoe, J.; Heremans, P. *Nat. Mater.* **2005**, *4*, 597.
(31) Rotzoll, R.; Mohapatra, S.; Olariu, V.; Wenz, R.; Grigas, M.; Dimmler, K.; Shchekin, O.; Dodabalapur, A. *Appl. Phys. Lett.* **2006**, *88*, 123502.
(32) Someya, T.; Kato, Y.; Sekitani, T.; Iba, S.; Noguchi, Y.; Murase, Y.; Kawaguchi, H.; Sakurai, T. *Proc. Natl. Acad. Sci. U.S.A.* **2005**, *102*, 12321.
(33) Khan, H. U.; Roberts, M. E.; Johnson, O.; Förch, R.; Knoll, W.; Bao, Z. *Adv. Mater.* **2010**, *22*, 4452.
(34) Zou, Y.; Najari, A.; Berrouard, P.; Beaupré, S.; Réda Aïch, B.; Tao, Y.; Leclerc, M. *J. Am. Chem. Soc.* **2010**, *132*, 5330.
(35) Piliego, C.; Holcombe, T. W.; Douglas, J. D.; Woo, C. H.; Beaujuge, P. M.; Fréchet, J. M. J. *J. Am. Chem. Soc.* **2010**, *132*, 7595.
(36) Zhang, Y.; Hau, S. K.; Yip, H.-L.; Sun, Y.; Acton, O.; Jen, A. K. Y. *Chem. Mater.* **2010**, *22*, 2696.
(37) Zhang, G.; Fu, Y.; Zhang, Q.; Xie, Z. *Chem. Commun.* **2010**, *46*, 4997.
(38) Yuan, M.-C.; Chiu, M.-Y.; Liu, S.-P.; Chen, C.-M.; Wei, K.-H. *Macromolecules* **2010**, *43*, 6936.
(39) Najari, A.; Beaupré, S.; Berrouard, P.; Zou, Y.; Pouliot, J.-R.; Lepage-Pérusse, C.; Leclerc, M. *Adv. Funct. Mater.* **2011**, *21*, 718.
(40) Guo, X.; Xin, H.; Kim, F. S.; Liyanage, A. D. T.; Jenekhe, S. A.; Watson, M. D. *Macromolecules* **2011**, *44*, 269.
(41) Zhang, Y.; Zou, J.; Yip, H.-L.; Sun, Y.; Davies, J. A.; Chen, K.-S.; Acton, O.; Jen, A. K. Y. *J. Mater. Chem.* **2011**, *21*, 3895.
(42) Hong, Y.-R.; Wong, H.-K.; Moh, L. C. H.; Tan, H.-S.; Chen, Z.-K. *Chem. Commun.* **2011**, *47*, 4920.
(43) Chen, G.-Y.; Cheng, Y.-H.; Chou, Y.-J.; Su, M.-S.; Chen, C.-M.; Wei, K.-H. *Chem. Commun.* **2011**, *47*, 5064.
(44) Griffini, G.; Douglas, J. D.; Piliego, C.; Holcombe, T. W.; Turri, S.; Fréchet, J. M. J.; Mynar, J. L. *Adv. Mater.* **2011**, *23*, 1660.
(45) Chu, T.-Y.; Lu, J.; Beaupré, S.; Zhang, Y.; Pouliot, J.-R.; Wakim, S.; Zhou, J.; Leclerc, M.; Li, Z.; Ding, J.; Tao, Y. *J. Am. Chem. Soc.* **2011**, *133*, 4250.
(46) Usta, H.; Lu, G.; Facchetti, A.; Marks, T. J. *J. Am. Chem. Soc.* **2006**, *128*, 9034.
(47) Ahmed, E.; Kim, F. S.; Xin, H.; Jenekhe, S. A. *Macromolecules* **2009**, *42*, 8615.
(48) Lu, G.; Usta, H.; Risko, C.; Wang, L.; Facchetti, A.; Ratner, M. A.; Marks, T. J. *J. Am. Chem. Soc.* **2008**, *130*, 7670.
(49) Facchetti, A. *Chem. Mater.* **2011**, *23*, 733.
(50) Letizia, J. A.; Salata, M. R.; Tribout, C. M.; Facchetti, A.; Ratner, M. A.; Marks, T. J. *J. Am. Chem. Soc.* **2008**, *130*, 9679.
(51) Guo, X.; Ortiz, R. P.; Zheng, Y.; Hu, Y.; Noh, Y.-Y.; Baeg, K.-J.; Facchetti, A.; Marks, T. J. *J. Am. Chem. Soc.* **2011**, *133*, 1405.
(52) Nielsen, C. B.; Bjørnholm, T. *Org. Lett.* **2004**, *6*, 3381.
(53) Pomerantz, M. *Tetrahedron Lett.* **2003**, *44*, 1563.
(54) Guo, X.; Watson, M. D. *Org. Lett.* **2008**, *10*, 5333.
(55) Guo, X.; Kim, F. S.; Jenekhe, S. A.; Watson, M. D. *J. Am. Chem. Soc.* **2009**, *131*, 7206.
(56) Hergué, N.; Mallet, C.; Savitha, G.; Allain, M.; Frère, P.; Roncali, J. *Org. Lett.* **2011**, *13*, 1762.
(57) Zhang, Q.; Tour, J. M. *J. Am. Chem. Soc.* **1997**, *119*, 5065.

(58) Baklar, M.; Wobkenberg, P. H.; Sparrowe, D.; Goncalves, M.; McCulloch, I.; Heeney, M.; Anthopoulos, T.; Stingelin, N. *J. Mater. Chem.* **2010**, *20*, 1927.
(59) Baeg, K.-J.; Khim, D.; Kim, D.-Y.; Jung, S.-W.; Koo, J. B.; You, I.-K.; Yan, H.; Facchetti, A.; Noh, Y.-Y. *J. Polym. Sci., Part B: Polym. Phys.* **2011**, *49*, 62.
(60) Berrouard, P.; Grenier, F.; Pouliot, J. R.; Gagnon, E.; Tessier, C.; Leclerc, M. *Org. Lett.* **2011**, *13*, 38.
(61) Lens, M.; Koster, L. J. A.; Mihailetchi, V. D.; Blom, P. W. M. *Appl. Phys. Lett.* **2006**, *88*, 243502.
(62) Wu, P.-T.; Xin, H.; Kim, F. S.; Ren, G.; Jenekhe, S. A. *Macromolecules* **2009**, *42*, 8817.
(63) Leenen, M. A. M.; Meyer, T.; Cucinotta, F.; Thiem, H.; Anselmann, R.; De Cola, L. *J. Polym. Sci., Part A: Polym. Chem.* **2010**, *48*, 1973.
(64) Li, J.; Tan, H. S.; Chen, Z. K.; Goh, W. P.; Wong, H. K.; Ong, K. H.; Liu, W.; Li, C. M.; Ong, B. S. *Macromolecules* **2011**, *44*, 690.
(65) He, M.; Li, J.; Sorensen, M. L.; Zhang, F.; Hancock, R. R.; Fong, H. H.; Pozdin, V. A.; Smilgies, D. M.; Malliaras, G. G. *J. Am. Chem. Soc.* **2009**, *131*, 11930.
(66) Ong, B. S.; Wu, Y.; Liu, P.; Gardner, S. *J. Am. Chem. Soc.* **2004**, *126*, 3378.
(67) Murphy, A. R.; Liu, J. S.; Luscombe, C.; Kavulak, D.; Fréchet, J. M. J.; Kline, R. J.; McGehee, M. D. *Chem. Mater.* **2005**, *17*, 4892.
(68) Meerholz, K.; Heinze, J. *Electrochim. Acta* **1996**, *41*, 1839.
(69) Sauve, G.; Javier, A. E.; Zhang, R.; Liu, J. Y.; Sydlik, S. A.; Kowalewski, T.; McCullough, R. D. *J. Mater. Chem.* **2010**, *20*, 3195.
(70) Kim, J.; Swager, T. M. *Nature* **2001**, *411*, 1030.
(71) Newman, C. R.; Frisbie, C. D.; da Silva, D. A.; Bredas, J. L.; Ewbank, P. C.; Mann, K. R. *Chem. Mater.* **2004**, *16*, 4436.
(72) Park, J. K.; Jo, J.; Seo, J. H.; Moon, J. S.; Park, Y. D.; Lee, K.; Heeger, A. J.; Bazan, G. C. *Adv. Mater.* **2011**, *23*, 2430.
(73) Durban, M. M.; Kazarinoff, P. D.; Luscombe, C. K. *Macromolecules* **2010**, *43*, 6348.
(74) Dimitrakopoulos, C. D.; Malenfant, P. R. L. *Adv. Mater.* **2002**, *14*, 99.
(75) Osaka, I.; McCullough, R. D. *Acc. Chem. Res.* **2008**, *41*, 1202–1214.
(76) Ong, K. H.; Lim, S. L.; Tan, H. S.; Wong, H. K.; Li, J.; Ma, Z.; Moh, L. C. H.; Lim, S. H.; De Mello, J. C.; Chen, Z. K. *Adv. Mater.* **2011**, *23*, 1409.
(77) Hwang, D. K.; Fuentes-Hernandez, C.; Kim, J.; Potscavage, W. J.; Kim, S.-J.; Kippelen, B. *Adv. Mater.* **2011**, *23*, 1293.
(78) DiBenedetto, S. A.; Facchetti, A.; Ratner, M. A.; Marks, T. J. *Adv. Mater.* **2009**, *21*, 1407.
(79) Ortiz, R. P.; Facchetti, A.; Marks, T. J. *Chem. Rev.* **2010**, *110*, 205.